

PROTOSTELLAR FEEDBACK AND FINAL MASS  
 OF THE SECOND-GENERATION PRIMORDIAL STARS

TAKASHI HOSOKAWA<sup>1,2</sup>, NAOKI YOSHIDA<sup>1,3</sup>, KAZUYUKI OMUKAI<sup>4</sup>, HAROLD W. YORKE<sup>2</sup>

*Draft version July 9, 2018*

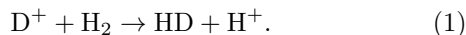
ABSTRACT

The first stars in the universe ionized the ambient primordial gas through various feedback processes. “Second-generation” primordial stars potentially form from this disturbed gas after its recombination. In this *Letter*, we study the late formation stage of such second-generation stars, where a large amount of gas accretes onto the protostar and the final stellar mass is determined when the accretion terminates. We directly compute the complex interplay between the accretion flow and stellar ultraviolet (UV) radiation, performing radiation-hydrodynamic simulations coupled with stellar evolution calculations. Because of more efficient H<sub>2</sub> and HD cooling in the pre-stellar stage, the accretion rates onto the star are ten times lower than in the case of the formation of the first stars. The lower accretion rates and envelope density result in the occurrence of an expanding bipolar HII region at a lower protostellar mass  $M_* \simeq 10M_\odot$ , which blows out the circumstellar material, thereby quenching the mass supply from the envelope to the accretion disk. At the same time the disk loses mass due to photoevaporation by the growing star. In our fiducial case the stellar UV feedback terminates mass accretion onto the star at  $M_* \simeq 17 M_\odot$ . Although the derived masses of the second-generation primordial stars are systematically lower than those of the first generation, the difference is within a factor of only a few. Our results suggest a new scenario, whereby the majority of the primordial stars are born as massive stars with tens of solar masses, regardless of their generations.

*Subject headings:* cosmology: theory – early universe – stars: formation – stars: evolution – accretion – HII regions

1. INTRODUCTION

Standard cosmology predicts that the cradles of the very first stars in the universe are massive (100 – 1000  $M_\odot$ ) gas clumps formed in minihalos hundreds million years after the Big Bang (e.g., Abel et al. 2002; Bromm et al. 2002; Yoshida et al. 2003). The massive primordial stars ionize their natal clouds by ultraviolet (UV) radiation. If these stars die without triggering supernova explosions, their relic HII regions, where the ionized gas recombined subsequently, become a promising site for the formation of second-generation stars (e.g., Oh & Haiman 2003). The pre-stellar thermal evolution of these second-generation stars differs from that of the very first stars. The enhanced free electrons, catalysts for forming H<sub>2</sub> molecules, in the relic HII regions results in the higher H<sub>2</sub> abundance than in the case of the first stars. The higher H<sub>2</sub> abundance enables the production of cold ( $\lesssim 150$  K) dense gas, where most of the deuterium is converted to molecular form (e.g., Uehara & Inutsuka 2000; Nakamura & Umemura 2002; Nagakura & Omukai 2005; Johnson & Bromm 2006) by the exothermic reaction



With the additional radiative cooling via HD molecules, the temperature further falls to a few  $\times 10$  K, which is close to the CMB temperature at high redshifts. By contrast, in the case of first-star formation the temperature remains  $\gtrsim 200$ K. Strong shocks or cosmic-rays can raise the ionization degree of a primordial gas, thereby setting similar physical conditions (e.g., Stacy & Bromm 2007; Safronek-Shrader et al. 2010; Inayoshi & Omukai 2011; Omukai 2012). The typical mass of the star-forming clouds is given by the Jeans mass when the contracting gas attains its minimum temperature

$$M_c \sim M_J \simeq 70 M_\odot \left( \frac{n}{10^5 \text{cm}^{-3}} \right)^{-1/2} \left( \frac{T}{50 \text{K}} \right)^{3/2}, \quad (2)$$

where the characteristic density and temperature are set by the HD cooling (e.g., O’Shea et al. 2005; Yoshida et al. 2007a; McGreer & Bryan 2008). This cloud mass-scale is about an order of magnitude less massive than that for the formation of the very first stars:

$$M_c \sim M_J \simeq 2000 M_\odot \left( \frac{n}{10^4 \text{cm}^{-3}} \right)^{-1/2} \left( \frac{T}{200 \text{K}} \right)^{3/2}, \quad (3)$$

where the characteristic density and temperature are set by the H<sub>2</sub> cooling (Bromm et al. 1999).

Because of the difference in the mass-scale of their natal clouds, the first- and second-generation primordial stars have been classified into different sub-populations: Population III.1 (Pop III.1) and III.2 (Pop III.2) stars (e.g., O’Shea et al. 2008). Until recently, the standard picture of primordial star formation postulated very massive (a few  $\times 100 M_\odot$ ) Pop III.1 stars and less massive Pop III.2 stars (a few  $\times 10 M_\odot$ ). However, their final stel-

<sup>1</sup>Department of Physics, University of Tokyo, Tokyo 113-0033, Japan; takashi.hosokawa@phys.s.u-tokyo.ac.jp, hosokwtk@gmail.com

<sup>2</sup>Jet Propulsion Laboratory, California Institute of Technology, Pasadena CA 91109, USA

<sup>3</sup>Kavli Institute for the Physics and Mathematics of the Universe, University of Tokyo, Kashiwa, Chiba 277-8583, Japan

<sup>4</sup>Department of Physics, Kyoto University, Kyoto 606-8502, Japan

TABLE 1  
INCLUDED DEUTERIUM CHEMISTRY

No.	Reactions	References
R1	$D^+ + e \rightarrow D + \gamma$	1
R2	$D + H^+ \rightarrow D^+ + H$	1
R3	$D^+ + H \rightarrow D + H^+$	1
R4	$D + H \rightarrow HD + \gamma$	2
R5	$D + H_2 \rightarrow H + HD$	3
R6	$D^+ + H_2 \rightarrow H^+ + HD$	2
R7	$HD + H \rightarrow H_2 + D$	2
R8	$HD + H^+ \rightarrow H_2 + D^+$	2
R9	$HD + \gamma \rightarrow H + D$	4

NOTE. — 1: Galli & Palla (1998), 2: Stancil et al. (1998), 3: Wang & Stancil (2002), 4: Wolcott-Green & Haiman (2011)

lar masses are still not clear. Both in the Pop III.1 and III.2 cases, very small ( $\simeq 0.01 M_\odot$ ) embryo protostars form after the gravitational collapse of the natal clouds (e.g., Omukai & Nishi 1998; Yoshida et al. 2008). These protostars then rapidly grow in mass by accretion of gas from their surrounding envelopes. The final stellar mass is thought to be set when the mass accretion ceases.

The key physical mechanism that controls the final stellar mass is stellar radiation feedback against the accretion flow (e.g., McKee & Tan 2008; Hosokawa et al. 2011; Stacy et al. 2012). In our previous work (Hosokawa et al. 2011, hereafter H11), we have reported the first radiation-hydrodynamic simulations for the Pop III.1 case that cover the long-term ( $\simeq 10^5$  years) evolution after the birth of the embryo protostar. We have demonstrated that the strong stellar UV feedback indeed terminates protostellar accretion, and shown that the resulting final stellar mass is  $\simeq 40 M_\odot$ . This mass range of Pop III.1 stars is much lower than previously postulated and is rather close to that expected for Pop III.2 stars.

In this *Letter*, we apply the same method to a typical Pop III.2 star-forming cloud found in a cosmological simulation (Yoshida et al. 2007b). We find that although the final masses of Pop III.2 stars are systematically lower than those of Pop III.1 stars, the difference is by a factor of only a few. This result suggests that, whereas lower-mass stars potentially form as satellite-like objects via gravitational fragmentation of the star-forming cloud (e.g., Machida et al. 2008; Turk et al. 2009; Stacy et al. 2010; Clark et al. 2011), the majority of primordial stars are tens of solar masses regardless of their generations. The typical stellar systems in the early universe are likely to be such massive stars accompanied by a small number lower-mass satellite stars.

## 2. NUMERICAL METHOD

We employ the numerical method developed in H11 with necessary extensions. The hydrostatic evolution of the central protostar and the evolution of the accreting primordial gas are consistently solved (see H11 for details). The dynamics of the accretion flow is calculated with a two-dimensional (2D) axisymmetric radiation-hydrodynamics code (e.g., Yorke & Sonnhalter 2002; Yorke & Welz 1996). In addition to the chemical reactions implemented in H11, we also solve the deuterium chemistry with three species of D, HD, and  $D^+$  (Table 1). The HD-line cooling rate is calculated considering the first four rotational levels as in Galli & Palla

(1998). The central protostar is replaced with a sink cell, whose size is  $\simeq 10$  AU. This masking of the very vicinity of the star, where the gas density exceeds  $10^{11} \text{ cm}^{-3}$ , enables us to follow the long-term evolution. The mass accretion rate onto the protostar is evaluated from the mass influx to the sink cell. With the accretion rate provided, the protostellar evolution is calculated by solving the stellar interior structure numerically (e.g., Omukai & Palla 2003; Hosokawa & Omukai 2009). The stellar evolution then gives the stellar luminosity and effective temperature to the radiation hydrodynamics, which follows the interplay between the accretion flow and stellar radiation.

As in H11 we calculate the dynamics of the accretion flow within 0.3 pc of the protostar. The initial gas distribution is configured with the simulation output of Yoshida et al. (2007b), who study the formation of a protostellar core in a relic HII region, performing three-dimensional (3D) cosmological simulations. We reduce their 3D data at the moment when the central density reaches  $\simeq 10^{14} \text{ cm}^{-3}$  to 2D axisymmetric data by averaging over azimuthal angles. The original 3D data has some non-axisymmetric structure, but the deviation from the axial average is not large within the computational domain. Moreover, deviation from the axisymmetric structure is smaller in the inner part of the cloud. Our computational domain contains  $\simeq 150 M_\odot$ . Yoshida et al. (2007a,b) show that in the Pop III.2 case the mass of the cloud that experiences the dynamical run-away collapse is about  $40 M_\odot$ . In our initial condition, this part of the cloud is contained within 0.05 pc of the protostar. In comparison with the Pop III.1 case (H11), the density in the accreting envelope is lower, reflecting the lower temperature in the pre-stellar collapse stage. The grid resolution and boundary conditions are the same as in the fiducial case studied in H11.

## 3. RESULTS

Immediately after the onset of the calculation, the stellar mass increases rapidly by accretion via a circumstellar disk. The density within the disk is high enough ( $\gtrsim 10^8 \text{ cm}^{-3}$ ) for the three-body reaction to convert most of the H atoms to  $H_2$  molecules. This molecular disk extends to  $\simeq 500$  AU from the star when the stellar mass reaches  $5 M_\odot$ . The mass accretion rate onto the protostar decreases with increasing stellar mass, e.g.,  $1.7 \times 10^{-3} M_\odot \text{ yr}^{-1}$  at  $M_* = 2 M_\odot$ , while  $6.1 \times 10^{-4} M_\odot \text{ yr}^{-1}$  at  $M_* = 5 M_\odot$ . These rates are about an order of magnitude lower than those in the Pop III.1 case, due to the lower density in the accreting envelope resulting from the lower gas temperature during the run-away collapse stage: for the collapse of a self-gravitating cloud, the accretion rate is given by  $\dot{M}_* \sim c_s^3/G \propto T^{1.5}$ , where  $c_s$  and  $T$  are the sound speed and gas temperature in the accreting envelope (Shu 1977). In the Pop III.2 case, as described above, the gas temperature is lower than in the Pop III.1 case because of the efficient radiative cooling via extra  $H_2$  and HD molecules.

Figure 1-(a) shows that, early on, the protostellar radius is  $30 - 40 R_\odot$  and decreases slightly as the accretion rate decreases. The protostellar evolution can be understood by comparing the two timescales, namely the

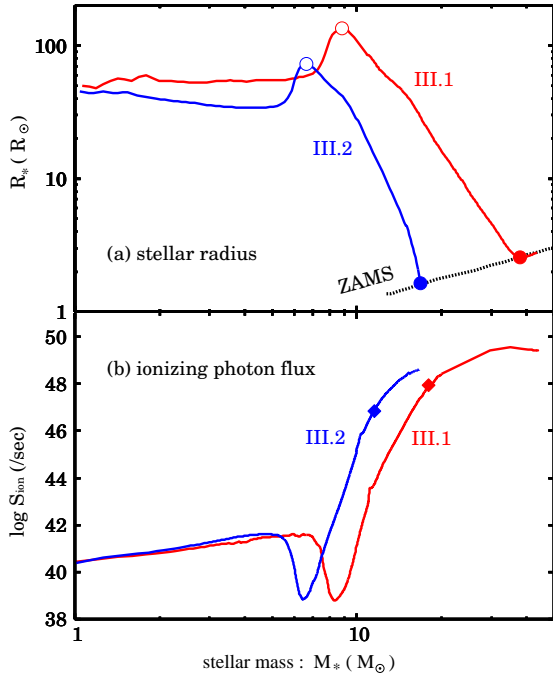


FIG. 1.— Evolution of the protostellar radius (*upper panel*) and ionizing ( $h\nu > 13.6$  eV) photon production rate (*lower panel*). The blue and red lines represent the fiducial Pop III.2 and III.1 cases in each panel. The black dotted line in the upper panel shows the mass-radius relation of metalless zero-age main-sequence stars. The open and filled circles mark the characteristic epochs of the protostellar evolution, beginning of the KH contraction and the arrival of the protostar to the ZAMS. The filled diamonds in the lower panel denote the epochs when the HII region begins to grow toward the polar directions of the disk.

stellar Kelvin-Helmholtz (KH) timescale

$$t_{\text{KH}} \equiv \frac{GM_* \dot{M}_*}{R_* L_*}, \quad (4)$$

and the accretion timescale

$$t_{\text{acc}} \equiv \frac{M_*}{\dot{M}_*}. \quad (5)$$

The former is the times over which the star radiates away its internal heat content, whereas the latter is the time over which the stellar mass doubles by accretion. Initially, the KH timescale is much longer than the accretion timescale, i.e., the star has no time to radiate its internal heat before its mass grows by accretion. This is the so-called adiabatic accretion stage (e.g., Stahler et al. 1986). Since the stellar luminosity  $L_*$  rises rapidly with increasing stellar mass, the KH timescale eventually falls below the accretion timescale at  $M_* \simeq 6 M_\odot$ , where the stellar radius marks its maximum. After this the protostar loses its internal heat efficiently by radiative diffusion and contracts quasi-hydrostatically (e.g., Omukai & Palla 2003). During this KH contraction stage the stellar effective temperature  $T_{\text{eff}}$  varies as  $\propto R_*^{-2}$  and H ionizing-photon ( $h\nu \geq 13.6$  eV) luminosity therefore increases significantly (Fig. 1-b).

After the stellar mass exceeds  $10 M_\odot$ , an HII region begins to develop, growing in the polar directions of the disk. Figure 2-(a) shows the gas distribution in the

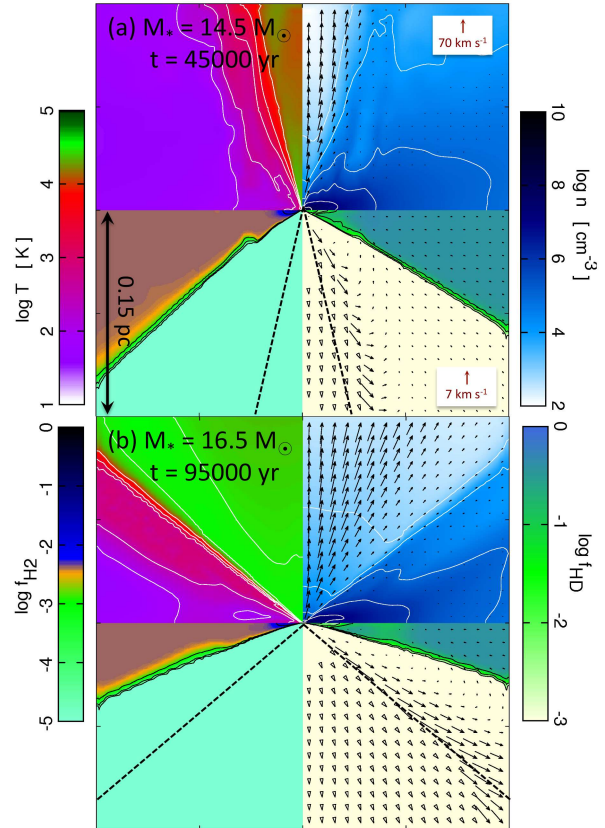


FIG. 2.— The structure of the accreting envelope surrounding the protostar. The panels (a) and (b) show the snapshots when the stellar mass is  $14.5 M_\odot$  and  $16.5 M_\odot$ , respectively. The elapsed time since the birth of the embryo protostar is also indicated on the upper-left corner. Each panel shows the spatial distributions of temperature (*upper left*), density (*upper right*), and molecular fractions of hydrogen (*lower left*) and deuterium (*lower right*). The arrows represent the velocity field with different scalings between the upper and lower panels. The open triangles in the lower panel indicate directions only for velocities higher than  $10.5$  km/sec. The dashed lines in the lower half of each panel define the edge of the HII region.

vicinity of the protostar at  $M_* = 14.5 M_\odot$ . We see that the bipolar HII region is breaking out from the accreting envelope.  $\text{H}_2$  and HD molecules are completely photodissociated by stellar  $\text{H}_2$  dissociating ( $11.2 \text{ eV} \leq h\nu \leq 13.6 \text{ eV}$ ) photons except in the shadow of the disk. Within the HII region the ionized gas flows outward at a velocity of several  $10$  km/s. The high pressure in the HII region drives a strong D-type shock, which compresses and heats up the surrounding materials to  $\sim 10^3$  K. The shocked gas has an outward velocity of several km/s. The HII region dynamically expands into the accretion envelope and its opening angle increases with protostellar mass (Fig. 2-b).

The growth of stellar mass via accretion continues even after the formation and initial expansion of the HII region. However, the accretion rate is reduced by radiative feedback when compared to the no-feedback case (Fig. 3). In contrast to the stellar UV radiation, the shock driven by the expanding HII region propagates around the disk and reaches the accreting envelope in the disk's shadow. The shocked gas flowing outward hinders accretion from the envelope onto the disk. The isolated disk exposed

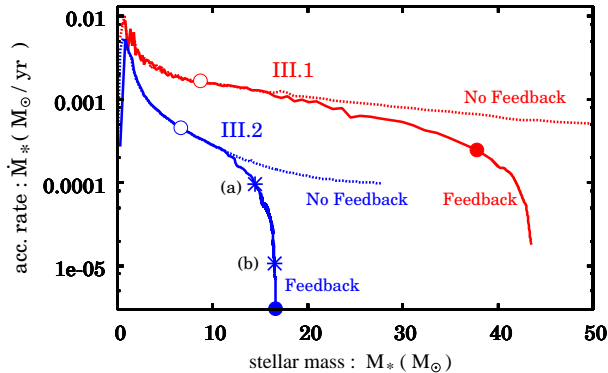


FIG. 3.— Evolution of the mass accretion rates onto the protostar. The blue solid curve represents the fiducial Pop III.2 case. The asterisks on this curve indicate the moments of the snapshots presented in Figure 2. The open and filled circles mark the characteristic epochs as in Figure 1. The blue dotted curve denotes the reference case, whereby the stellar UV feedback was switched off. The red solid and dotted curves represent the fiducial Pop III.1 cases with and without the stellar UV feedback taken from Hosokawa et al. (2011).

to the stellar UV radiation thins down via photoevaporation. Accretion from the disk onto the star finally terminates at  $M_* \simeq 16.6 M_\odot$ . This coincides with the moment when the protostar reaches the zero-age main-sequence stage (Fig. 1-b).

Although the above overall evolution is qualitatively similar to that of Pop III.1 stars (H11), the resultant final stellar mass  $M_* \simeq 16.6 M_\odot$  is lower than for the fiducial III.1 case  $\simeq 43 M_\odot$  (Figure 3). This is mostly due to the fact that the protostellar evolution differs with the different accretion histories between the Pop III.1 and III.2 cases (Fig. 1). At the lower accretion rate, in general, the KH timescale becomes comparable to the accretion timescale at a lower luminosity. The protostar thus begins to lose its internal energy and contracts at lower stellar mass (e.g., Omukai & Palla 2003; Hosokawa & Omukai 2009). The stellar ionizing luminosity significantly increases during the KH contraction stage. Therefore, the UV feedback is effective at a lower stellar mass in the Pop III.2 case. Although the mechanism of dynamical expansion of an HII region and subsequent photoevaporation of the disk, which ultimately shuts off the mass accretion, is common between the Pop III.1 and III.2 cases, the required stellar ionizing luminosity for this mechanism to operate is much lower in the Pop III.2 case than for the Pop III.1 case (Fig. 1-b). This is because the HII region expands more easily through the lower-density Pop III.2 accretion envelope. The accompanying protostellar outflow and photoevaporation rates are also smaller than in the Pop III.1 case. In the Pop III.2 case, however, the weak UV stellar feedback is enough to shut off the slow mass accretion toward the protostar.

#### 4. DISCUSSION

In this *Letter*, we have shown that radiative feedback limits the final mass of a “typical” Pop III.2 protostar to  $\lesssim 20 M_\odot$ . With all the possible variations of initial conditions among different primordial gas clouds, we naturally expect that the resulting final stellar masses

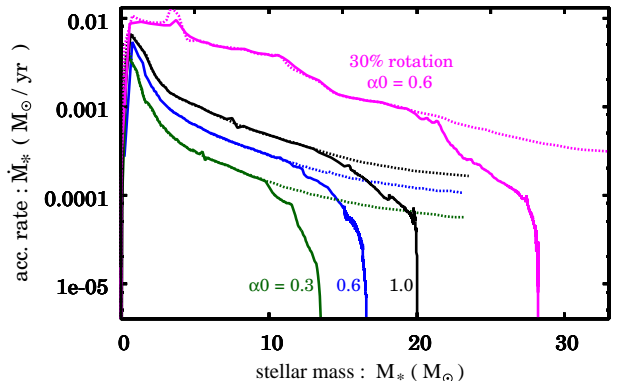


FIG. 4.— Evolution of the mass accretion rates onto the protostar with different parameters. The green, blue, and black lines represent the cases with different  $\alpha$ -viscosity parameters of  $\alpha_0 = 0.3, 0.6$  (fiducial case), and 1.0. The magenta lines denote the test cases where the rotation of the cloud is artificially reduced to 30% of the original values. The solid and dashed lines represent the evolution with and without the stellar UV feedback in each case.

would have some distribution. Cosmological simulations predict that, in the Pop III.1 case, the accretion rate onto a star could differ by more than two orders of magnitude among different star-forming clouds which form through various halo assembly histories (e.g., O’Shea & Norman 2007). Although such systematic studies have not been conducted for the Pop III.2 case, we expect a similar variance and hence some distribution of the final stellar masses. Here we examine potential variances of the final stellar masses in our simulations.

For instance, we use the  $\alpha$ -viscosity formalism (Shakura & Sunyaev 1973) for mimicking the torque exerted by non-axisymmetric spiral arms formed in massive self-gravitating disks (e.g., Yorke & Sonnhalter 2002; Kuiper et al. 2010). Recent 3D simulations show that the effective  $\alpha$ -parameter is around 0.1 – 1 in this case (e.g., Clark et al. 2011; Kuiper et al. 2011); we adopt an  $\alpha$ -parameter in the mid-plane  $\alpha_0 = 0.6$  (see H11) for the fiducial case discussed above. Figure 4 shows the accretion histories and resulting final stellar masses for different values of  $\alpha_0$ . Analogously to H11, the final stellar mass increases with the value of  $\alpha_0$ :  $M_* \simeq 13.6 M_\odot$  for  $\alpha_0 = 0.3$ , whereas  $M_* \simeq 20.0 M_\odot$  for  $\alpha_0 = 1.0$ . Figure 4 also shows the cases where the initial rotation of the natal cloud is reduced to 30% of the fiducial value. For this case the stellar UV feedback operates only after 20  $M_\odot$  of the gas has accreted onto the star and the resulting final stellar mass is  $M_* \simeq 28 M_\odot$ .

Although this mass range is systematically lower than that of Pop III.1 stars derived in H11, the difference is within a factor of a few. In reality, the existence of photodissociating background radiation could further erase the difference in the final masses of Pop III.1 and III.2 stars. Recall that the lower masses of Pop III.2 stars originates from the enhanced abundances of  $H_2$  and HD, and the resultant more efficient cooling during the pre-stellar collapse of the natal cloud. However, the presence of even a weak photodissociating background ( $\sim 10^{-22} \text{ erg cm}^{-2} \text{ sr}^{-1} \text{ sec}^{-1} \text{ Hz}^{-1}$ ) inhibits the formation of  $H_2$  and HD molecules, thereby making the thermal evolution almost the same in the Pop III.1 case (e.g.,

Yoshida et al. 2007b; Wolcott-Green & Haiman 2011). If this is the case, the mass scale of Pop III.1 and III.2 stars would be identical.

Although not considered in this study, gravitational fragmentation of the disk would also contribute to shape the mass distribution of primordial stars. For the Pop III.1 case, recent 3D numerical simulations show that the circumstellar disk easily becomes gravitationally unstable to fragmentation (e.g., Machida et al. 2008; Stacy et al. 2010; Clark et al. 2011; Greif et al. 2012). However, most of these studies consider the early evolution only, far before the mass accretion ceases and final stellar masses are determined. One can naively expect that disk fragmentation reduces the final stellar mass as the accreting material is shared by multiple protostars born from the fragments (so-called "fragmentation-induced starvation", e.g., Peters et al. 2010).

The nature of mass accretion with disk fragmentation might be even more complex during later evolutionary phases. For instance, gravitational interactions between the multiple protostars could redistribute angular momentum. If angular momentum is carried away by a small number of (proto-)stars thrown out of the system, accretion of the remaining gas onto the remaining star(s) could be enhanced. Moreover, merging of protostars in the disk is also possible. The net result is that mass accretion onto the star would be strongly time-dependent or even have the consequence of stochastic burst-like accretion events which potentially change the evolution of the protostars (but see, e.g., Smith et al. 2012). These effects should be examined in future long-term 3D simu-

lations.

If some of the low-mass stars born via the disk fragmentation survive without significant mass growth, they would be low-mass satellite-like stars orbiting around the massive stars whose final masses are limited by stellar radiative feedback. Future work would explain how this effect differs between the Pop III.1 and III.2 cases (e.g., Machida et al. 2009). As shown in Clark et al. (2011), disk fragmentation is controlled by a balance between the mass transfer rates onto and through the disk. Systematic difference in accretion rates onto the star-disk systems among the Pop III.1 and III.2 cases would result in basic differences in the effects of disk fragmentation.

Our results provide a new picture that the typical mass of the primordial stars are tens of solar masses regardless of their generations. This explains why the signatures of pair-instability supernova, which is the final fate of  $140 M_{\odot} \lesssim M_{*} \lesssim 260 M_{\odot}$  stars, have not been seen in the abundance patterns of Galactic metal-poor stars (e.g., Tumlinson et al. 2004; Frebel et al. 2009; Caffau et al. 2011).

The authors thank Neal Turner and Rolf Kuiper for fruitful discussions and comments. T.H. appreciates the support by Fellowship of the Japan Society for the Promotion of Science for Research Abroad. K.O. is supported by the Grants-in-Aid by the Ministry of Education, Science and Culture of Japan (2168407 and 21244021). Portions of this work were conducted at the Jet Propulsion Laboratory, California Institute of Technology, operating under a contract with the National Aeronautics and Space Administration (NASA).

## REFERENCES

- Abel, T., Bryan, G. L., & Norman, M. L. 2002, *Science*, 295, 93  
 Bromm, V., Coppi, P. S., & Larson, R. B. 1999, *ApJ*, 527, L5  
 —. 2002, *ApJ*, 564, 23  
 Caffau, E., et al. 2011, *Nature*, 477, 67  
 Clark, P. C., Glover, S. C. O., Smith, R. J., Greif, T. H., Klessen, R. S., & Bromm, V. 2011, *Science*, 331, 1040  
 Frebel, A., Johnson, J. L., & Bromm, V. 2009, *MNRAS*, 392, L50  
 Gallii, D., & Palla, F. 1998, *A&A*, 335, 403  
 Greif, T. H., Bromm, V., Clark, P. C., Glover, S. C. O., Smith, R. J., Klessen, R. S., Yoshida, N., & Springel, V. 2012, *MNRAS*, 424, 399  
 Hosokawa, T., & Omukai, K. 2009, *ApJ*, 691, 823  
 Hosokawa, T., Omukai, K., Yoshida, N., & Yorke, H. W. 2011, *Science*, 334, 1250  
 Inayoshi, K., & Omukai, K. 2011, *MNRAS*, 416, 2748  
 Johnson, J. L., & Bromm, V. 2006, *MNRAS*, 366, 247  
 Kuiper, R., Klahr, H., Beuther, H., & Henning, T. 2010, *ApJ*, 722, 1556  
 —. 2011, *ApJ*, 732, 20  
 Machida, M. N., Omukai, K., & Matsumoto, T. 2009, *ApJ*, 705, 64  
 Machida, M. N., Omukai, K., Matsumoto, T., & Inutsuka, S.-i. 2008, *ApJ*, 677, 813  
 McGreer, I. D., & Bryan, G. L. 2008, *ApJ*, 685, 8  
 McKee, C. F., & Tan, J. C. 2008, *ApJ*, 681, 771  
 Nagakura, T., & Omukai, K. 2005, *MNRAS*, 364, 1378  
 Nakamura, F., & Umemura, M. 2002, *ApJ*, 569, 549  
 Oh, S. P., & Haiman, Z. 2003, *MNRAS*, 346, 456  
 Omukai, K. 2012, *ArXiv e-prints*, astro-ph/1205.0086  
 Omukai, K., & Nishi, R. 1998, *ApJ*, 508, 141  
 Omukai, K., & Palla, F. 2003, *ApJ*, 589, 677  
 O’Shea, B. W., Abel, T., Whalen, D., & Norman, M. L. 2005, *ApJ*, 628, L5  
 O’Shea, B. W., McKee, C. F., Heger, A., & Abel, T. 2008, in *American Institute of Physics Conference Series*, Vol. 990, First Stars III, ed. B. W. O’Shea & A. Heger, D13  
 O’Shea, B. W., & Norman, M. L. 2007, *ApJ*, 654, 66  
 Peters, T., Klessen, R. S., Mac Low, M.-M., & Banerjee, R. 2010, *ApJ*, 725, 134  
 Safranek-Shrader, C., Bromm, V., & Milosavljević, M. 2010, *ApJ*, 723, 1568  
 Shakura, N. I., & Sunyaev, R. A. 1973, *A&A*, 24, 337  
 Shu, F. H. 1977, *ApJ*, 214, 488  
 Smith, R. J., Hosokawa, T., Omukai, K., Glover, S. C. O., & Klessen, R. S. 2012, *MNRAS*, 424, 457  
 Stacy, A., & Bromm, V. 2007, *MNRAS*, 382, 229  
 Stacy, A., Greif, T. H., & Bromm, V. 2010, *MNRAS*, 403, 45  
 —. 2012, *MNRAS*, 422, 290  
 Stahler, S. W., Palla, F., & Salpeter, E. E. 1986, *ApJ*, 302, 590  
 Stancil, P. C., Lepp, S., & Dalgarno, A. 1998, *ApJ*, 509, 1  
 Tumlinson, J., Venkatesan, A., & Shull, J. M. 2004, *ApJ*, 612, 602  
 Turk, M. J., Abel, T., & O’Shea, B. 2009, *Science*, 325, 601  
 Uehara, H., & Inutsuka, S.-i. 2000, *ApJ*, 531, L91  
 Wang, J. G., & Stancil, P. C. 2002, *Phys. Scr. T*, 96, 72  
 Wolcott-Green, J., & Haiman, Z. 2011, *MNRAS*, 412, 2603  
 Yorke, H. W., & Sonnhalter, C. 2002, *ApJ*, 569, 846  
 Yorke, H. W., & Welz, A. 1996, *A&A*, 315, 555  
 Yoshida, N., Abel, T., Hernquist, L., & Sugiyama, N. 2003, *ApJ*, 592, 645  
 Yoshida, N., Oh, S. P., Kitayama, T., & Hernquist, L. 2007a, *ApJ*, 663, 687  
 Yoshida, N., Omukai, K., & Hernquist, L. 2007b, *ApJ*, 667, L117  
 —. 2008, *Science*, 321, 669